Unique solubility of polyoxoniobate salts in methanol: coordination to cations and POM methylation

P. A. Abramov*,[a,b] C. Vicent,[c] N. B. Kompankov,[a] J. A. Laricheva,[a] M. N. Sokolov[a,b]

Supporting information

Fig. S1. ESI-MS data for the solution of $[\{Cp^*Ir\}_2Nb_6O_{19}]^{4-}$ in MeOH.

Fig. S2. ESI-MS data for the solution of $[\{Cp^*Ir\}_2Ta_6O_{19}]^{4-}$ in H_2O and MeOH.

Table S1. Summary of the species detected upon dissolving hexametalate sample solutions in CH_3OH

Fig. S3. Building block of the crystal structure of **1**. C_6H_6 rings are omitted for clarity.

Fig. S4. Infinite channels in the crystal structure of **1** along [100] crystal direction.

Fig. S5. Chain-like potassium polycation in the crystal packing of **2**.

Fig. S6. Chain-like potassium polycation in the crystal packing of **3**.

Fig. S7. The layer in the crystal structure of **3**.

Fig. S8. The layer in the crystal structure of **2.**

Fig. S9. Coordination of the cations by free $\{Nb_3O_3\}$ faces of $[\{Cp^*Rh\}_2Nb_6O_{19}]^{4-}$ anion in the crystal structure of **2**.

Fig. S10. Coordination of the cations by free $\{Nb_3O_3\}$ faces of $[\{Cp^*Ir\}_2Nb_6O_{19}]^{4-}$ anion in the crystal structure of **3** (left), H-bonds between MeOH and the anion (right).

Table S2. Experimental details

Table S3. Hirshfeld charges on $[Nb_6O_{19}]^{8-}$, its $\{Cp^*Ir\}^{2+}$-capped and methylated derivatives

Table S4. Comparison of energies between the three isomers of $[trans\text{-}\{Cp^*Ir\}_2Nb_6O_{18}(OCH_3)]^{3-}$

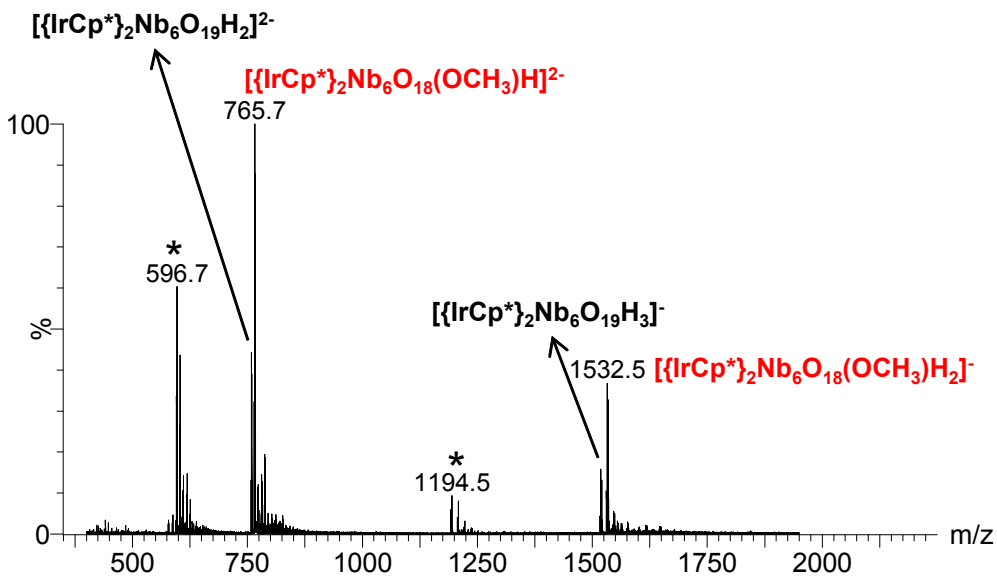

Fig. S1. ESI mass spectrum of methanol solutions of $[\{Cp^*Ir\}_2Nb_6O_{19}]^{4-}$. Species featuring methoxo groups are highlighted in red. Peaks depicted as * correspond to the 1:1 adducts derived from the $[\{Cp^*Ir\}Nb_6O_{19}]^{6-}$ anion.

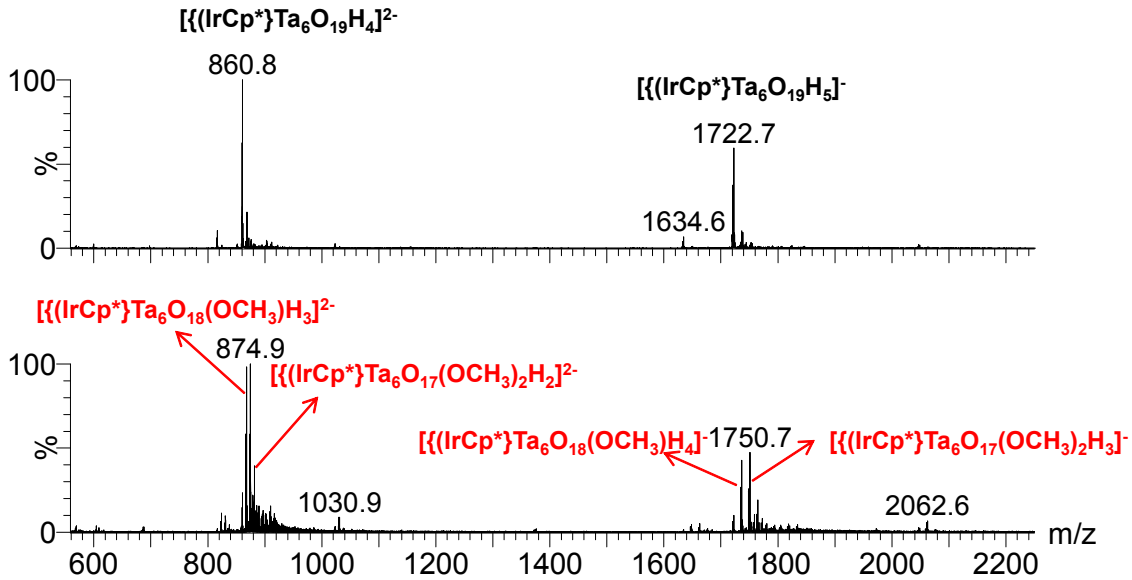

Fig. S2. ESI mass spectra of aqueous (top) and methanol (bottom) solutions of $[\{Cp^*Ir\}_2Ta_6O_{19}]^{4-}$ together with peak assignment. Species featuring methoxo groups are highlighted in red.

Table S1. Summary of the species detected upon dissolving hexametalate sample solutions in CH_3OH

Starting material	Identified species in the ESI mass spectra recorded in CH_3OH	m/z value
$K_4[(Cp^*Rh)_2Nb_6O_{19}]$	$([\{Cp^*Rh\}_2Nb_6O_{19}H_2]^{2-}$	669.7
	$([\{Cp^*Rh\}_2Nb_6O_{18}(OCH_3)H]^{2-}$	676.7
	$([\{Cp^*Rh\}_2Nb_6O_{19}H_3]^{-}$	1340.5
	$[\{Cp^*Rh\}_2Nb_6O_{18}(OCH_3)H_2]^{-}$	1354.5
$Cs_4[(Cp^*Rh)_2Ta_6O_{19}]$	$([\{Cp^*Rh\}_2Ta_6O_{19}H_2]^{2-}$	933.8
	$([\{Cp^*Rh\}_2Ta_6O_{18}(OCH_3)H]^{2-}$	940.8
	$([\{Cp^*Rh\}_2Ta_6O_{19}H_3]^{-}$	1868.6
	$[\{Cp^*Rh\}_2Ta_6O_{18}(OCH_3)H_2]^{-}$	1882.6
Reactions of $[Nb_6O_{19}]^{8-}$ with $[Cp^*RhCl_2]_2$ at the Rh/M_6 1:1 ratio	$([\{Cp^*Rh\}Nb_6O_{19}H_4]^{2-}$	551.7
	$[\{Cp^*Rh\}Nb_6O_{18}(OCH_3)H_3]^{2-}$	558.7
	$[\{Cp^*Rh\}Nb_6O_{17}(OCH_3)_2H_2]^{2-}$	565.7
	$([\{Cp^*Rh\}Nb_6O_{19}H_5]^{-}$	1104.4
	$[\{Cp^*Rh\}Nb_6O_{18}(OCH_3)H_4]^{-}$	1118.4
	$[\{Cp^*Rh\}Nb_6O_{17}(OCH_3)_2H_3]^{-}$	1132.4
Reactions of $[Ta_6O_{19}]^{8-}$ with $[Cp^*RhCl_2]_2$ at the Rh/M_6 1:1 ratio	$([\{Cp^*Rh\}Ta_6O_{19}H_4]^{2-}$	815.8
	$[\{Cp^*Rh\}Ta_6O_{18}(OCH_3)H_3]^{2-}$	822.8
	$[\{Cp^*Rh\}Ta_6O_{17}(OCH_3)_2H_2]^{2-}$	829.8
	$([\{Cp^*Rh\}Ta_6O_{19}H_5]^{-}$	1632.7
	$[\{Cp^*Rh\}Ta_6O_{18}(OCH_3)H_4]^{-}$	1646.7
	$[\{Cp^*Rh\}Ta_6O_{17}(OCH_3)_2H_3]^{-}$	1660.7
$Na_4[\{Cp^*Ir\}_2Nb_6O_{19}]$	$([\{Cp^*Ir\}_2Nb_6O_{19}H_2]^{2-}$	758.8
	$[\{Cp^*Ir\}_2Ta_6O_{18}(OCH_3)H]^{2-}$	765.7
	$([\{Cp^*Ir\}_2Nb_6O_{19}H_3]^{-}$	1518.6
	$[\{Cp^*Ir\}_2Ta_6O_{18}(OCH_3)H_2]^{-}$	1532.5
$Na_6[\{Cp^*Ir\}Ta_6O_{19}]$	$([\{Cp^*Ir\}Ta_6O_{19}H_4]^{2-}$	860.8
	$[\{Cp^*Rh\}Ta_6O_{18}(OCH_3)H_3]^{2-}$	867.8
	$[\{Cp^*Rh\}Ta_6O_{17}(OCH_3)_2H_2]^{2-}$	874.9
	$([\{Cp^*Ir\}Ta_6O_{19}H_5]^{-}$	1722.7
	$[\{Cp^*Rh\}Ta_6O_{18}(OCH_3)H_4]^{-}$	1736.7
	$[\{Cp^*Rh\}Ta_6O_{17}(OCH_3)_2H_3]^{-}$	1750.7

Fig. S3. Building block of the crystal structure of **1**. C_6H_6 rings are omitted for clarity. Lindqvist anions are colored in blue octahedra, ruthenium - orange, sodium – green.

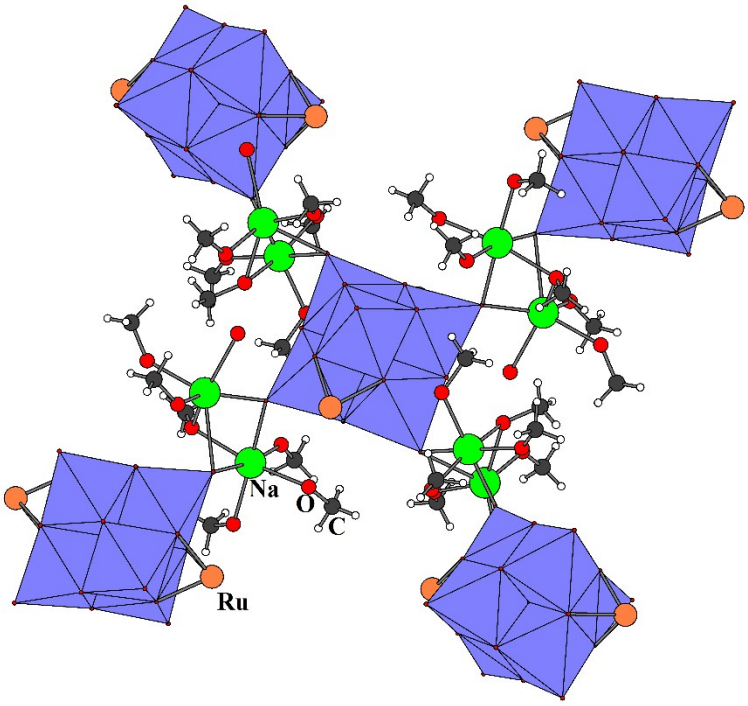

Fig. S4. Infinite channels in the crystal structure of **1** along [100] crystal direction. . Lindqvist anions are colored in blue octahedra, ruthenium - orange, sodium – green. Disordered solvate methanol molecules are omitted for clarity.

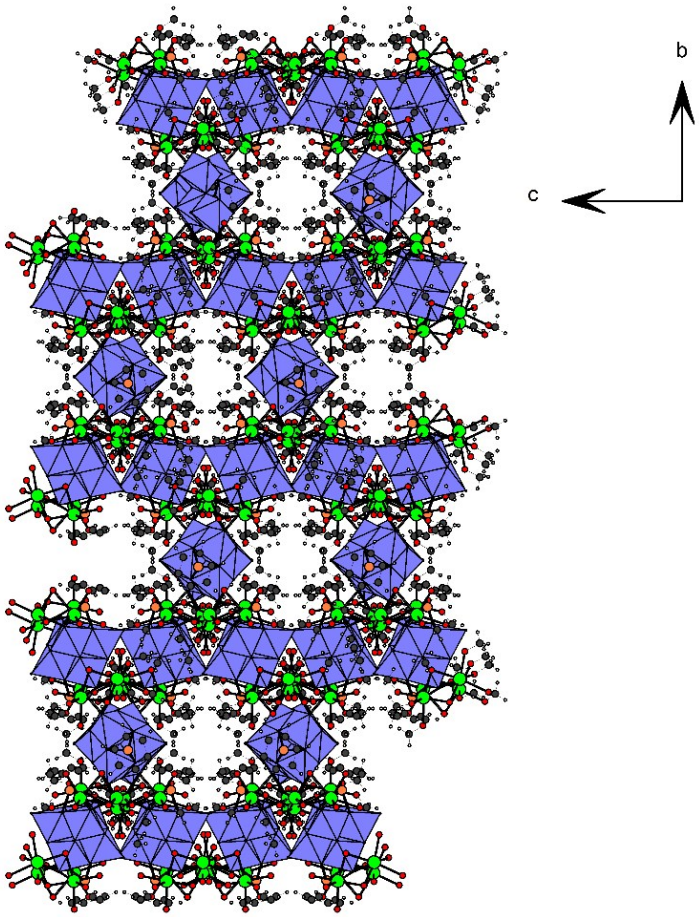

Fig. S5. Chain-like potassium polycation in the crystal packing of **2**. . Lindqvist anions are colored in blue octahedra, rhodium - orange, potassium – glaucous.

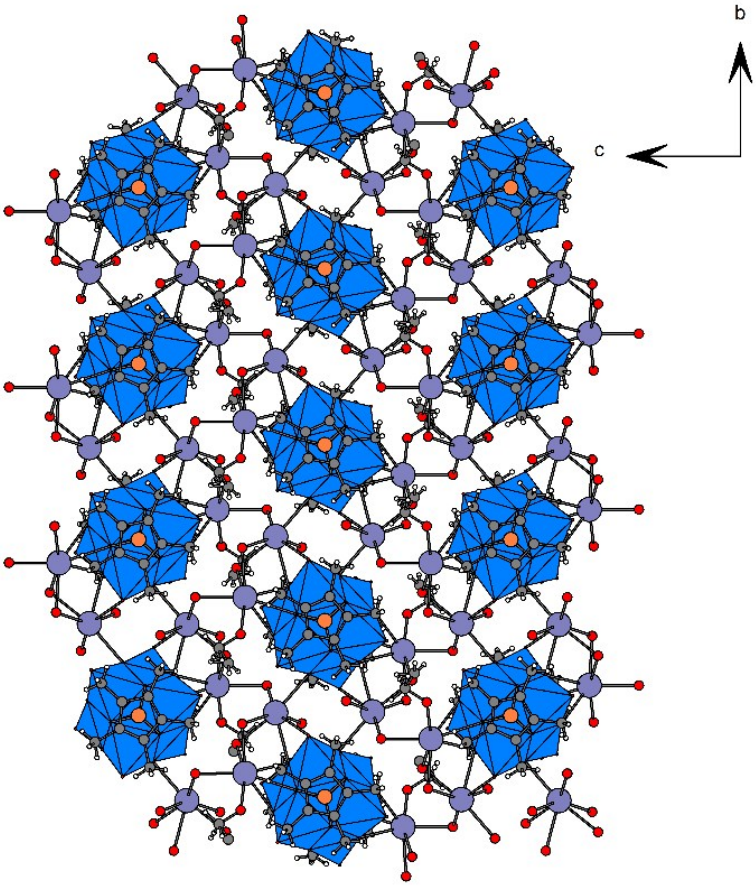

Fig. S6. Chain-like potassium polycation in the crystal packing of **3**. Niobium is blue, iridium is green, potassium is dark cyan.

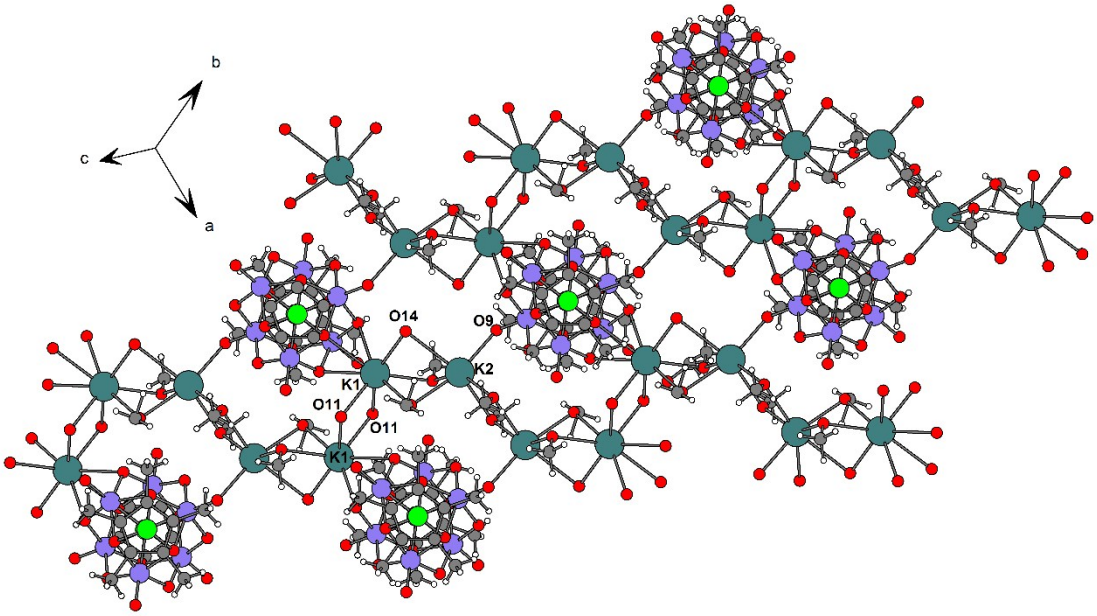

Fig. S7. The layer in the crystal structure of **3**. Niobium is blue, iridium is green, potassium is dark cyan.

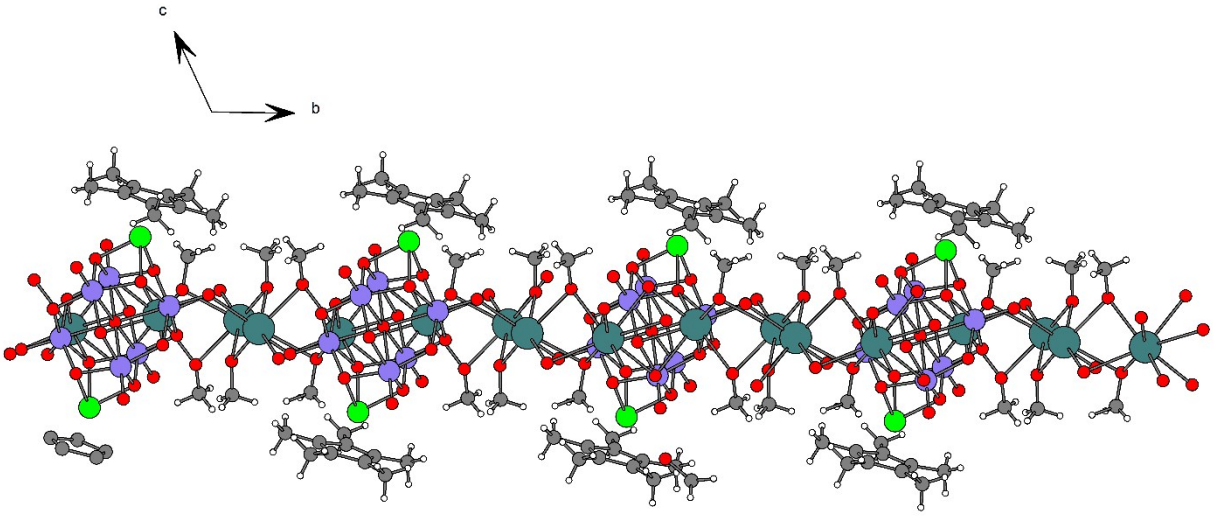

Fig. S8. The layer in the crystal structure of **2**. Lindqvist anions are colored in blue octahedra, rhodium - orange, potassium – glaucous.

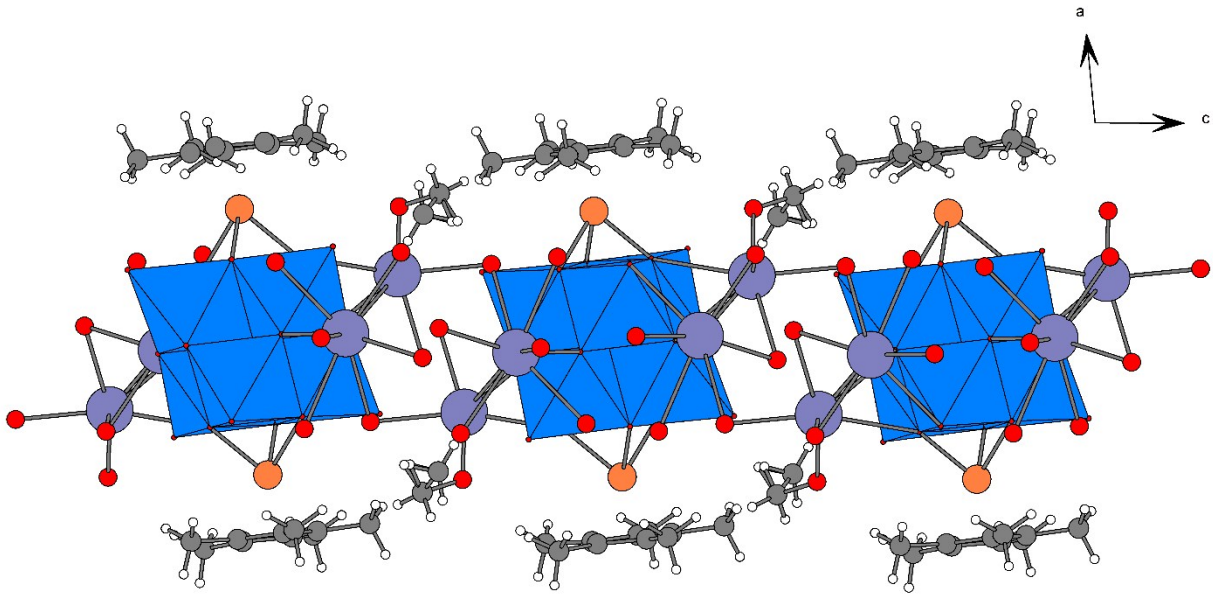

Fig. S9. Coordination of the cations by free $\{Nb_3O_3\}$ faces of $[\{Cp^*Rh\}_2Nb_6O_{19}]^{4-}$ anion in the crystal structure of **2**. Lindqvist anions are colored in blue octahedra, rhodium - orange, potassium – glaucous.

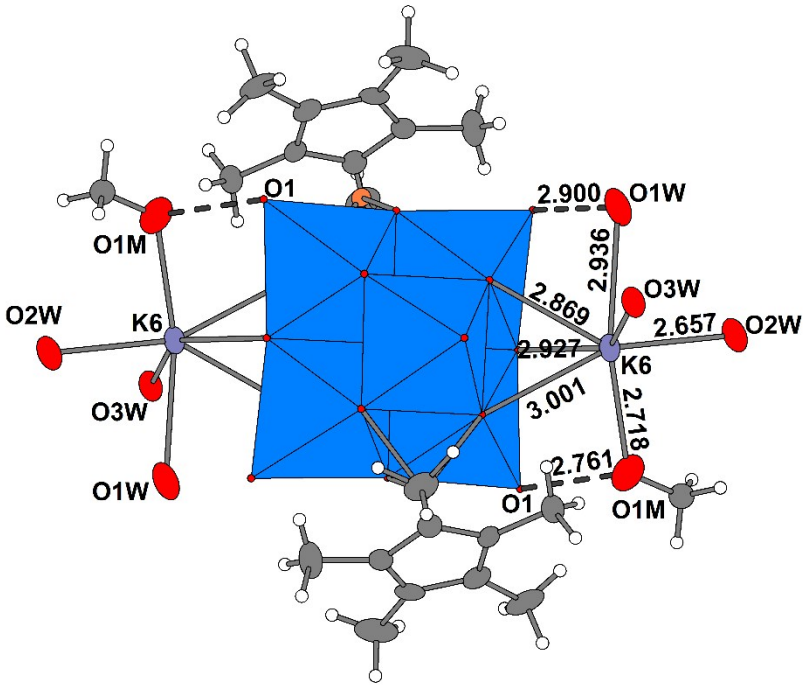

Fig. S10. Coordination of the cations by free $\{Nb_3O_3\}$ faces of $[\{Cp^*Ir\}_2Nb_6O_{19}]^{4-}$ anion in the crystal structure of **3** (left), H-bonds between MeOH and the anion (right). Niobium is blue, iridium is green, potassium is dark cyan.

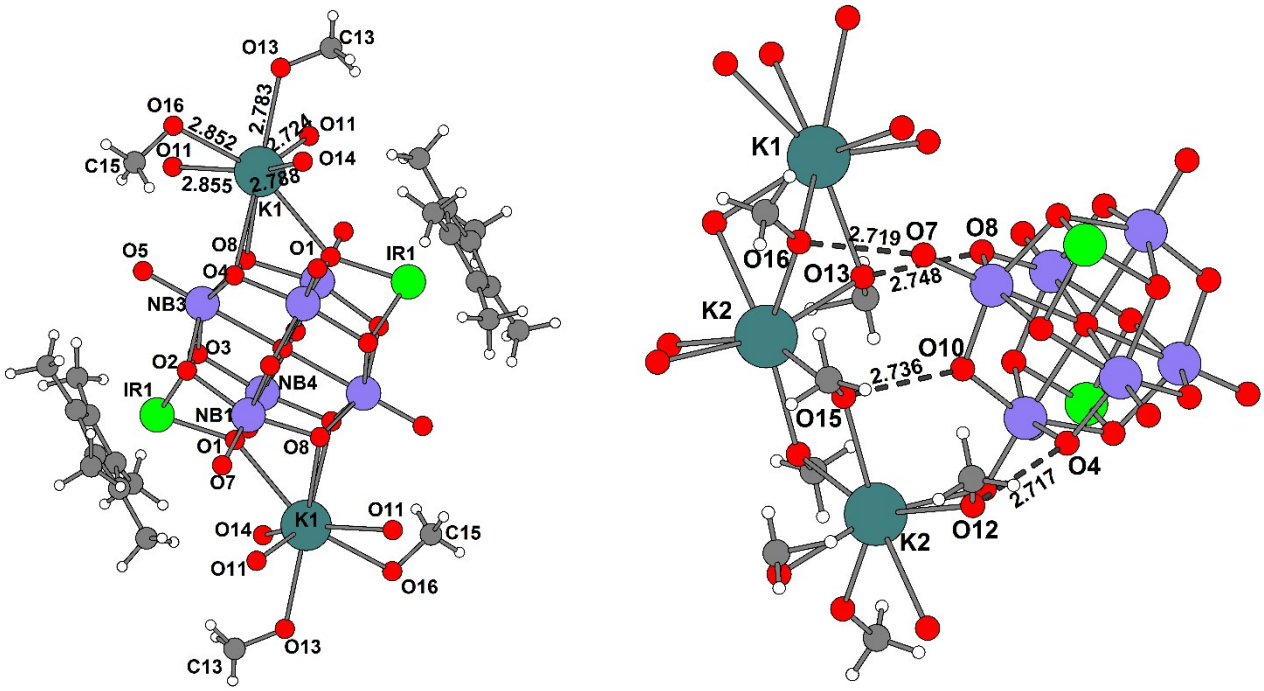

Table S2. Experimental details

	1	**2**	**3**
Chemical formula	$C_{26.12}H_{72.50}Na_4Nb_6O_{35.12}Ru_2$	$C_{30}H_{78}Ir_2K_4Nb_6O_{33}$	$C_{24}H_{66}K_4Nb_6O_{33}Rh_2$
M_r	1800.40	2065.18	1802.44
Crystal system, space group	Tetragonal, $I4_1/a$	Triclinic, $P\bar{1}$	Monoclinic, $P2_1/c$
a, b, c (Å)	30.105 (3), 30.105 (3), 14.0549 (13)	10.7760 (6), 11.8756 (7), 14.1839 (9)	14.6139 (5), 9.3769 (3), 19.9504 (5)
α, β, γ (°)	90, 90, 90	113.102 (3), 92.519 (3), 111.051 (2)	90, 95.964 (1), 90
V (Å^3)	12738 (3)	1521.58 (16)	2719.07 (14)
Z	8	1	2
μ (mm^{-1})	1.61	5.80	2.20
Crystal size (mm)	0.06 × 0.01 × 0.01	0.15 × 0.12 × 0.06	0.12 × 0.08 × 0.01
Diffractometer	Bruker Apex Duo	Bruker Nonius X8Apex CCD	Bruker Nonius X8Apex CCD
T_{min}, T_{max}	0.910, 0.981	0.477, 0.722	0.778, 0.974
No. of measured, independent and observed [$I > 2\sigma(I)$] reflections	26872, 6515, 5049	18012, 6901, 5935	17988, 6205, 4923
R_{int}	0.041	0.045	0.040
$(\sin \theta/\lambda)_{max}$ (Å^{-1})	0.625	0.651	0.650
$R[F^2 > 2\sigma(F^2)]$, $wR(F^2)$, S	0.035, 0.109, 1.05	0.033, 0.134, 1.16	0.040, 0.157, 1.14
No. of reflections, parameters, restraints	6515, 344, 0	6901, 344, 12	6205, 311, 0
H-atom treatment	H-atom parameters constrained	H atoms treated by a mixture of independent and constrained refinement	H-atom parameters constrained
	$w = 1/[\sigma^2(F_o^2) + (0.0528P)^2 + 99.642P]$ where $P = (F_o^2 + 2F_c^2)/3$	$w = 1/[\sigma^2(F_o^2) + (0.0764P)^2]$ where $P = (F_o^2 + 2F_c^2)/3$	$w = 1/[\sigma^2(F_o^2) + (0.0897P)^2 + 1.2721P]$ where $P = (F_o^2 + 2F_c^2)/3$
$\Delta\rangle_{max}$, $\Delta\rangle_{min}$ (e Å^{-3})	1.98, -0.78	1.70, -2.62	1.58, -2.81

Computer programs: *APEX2* (Bruker-AXS, 2004), *SAINT* (Bruker-AXS, 2004), *SHELXL2014*/7 (Sheldrick, 2014), SHELXLE (Sheldrick, 2011), CIFTAB-97 (Sheldrick, 2014).

Table S3. Hirshfeld charges on $[Nb_6O_{19}]^{8-}$, its $\{Cp^*Ir\}^{2+}$-capped and methylated derivatives.

$[Nb_6O_{19}]^{8-}$	$[\{Cp^*Ir\}Nb_6O_{19}]^{6-}$	[trans-$\{Cp^*Ir\}_2Nb_6O_{19}]^{4-}$	[cis-$\{Cp^*Ir\}_2Nb_6O_{19}]^{4-}$	[trans-$\{Cp^*Ir\}_2Nb_6O_{18}(OCH_3)]^{3-}$ Isomer I	[trans-$\{Cp^*Ir\}_2Nb_6O_{18}(OCH_3)]^{3-}$ Isomer II	[trans-$\{Cp^*Ir\}_2Nb_6O_{18}(OCH_3)]^{3-}$ Isomer III
-0.7542	-0.6197	-0.4904	-0.5224	-0.4605	-0.4563	-0.4427
0.4182	0.5919	0.6768	0.6662	0.6966	0.7078	0.7009
-0.3712	-0.4203	-0.4340	-0.4324	-0.4034	-0.4345	-0.4303
-0.4686	-0.4369	-0.3451	-0.4055	-0.3445	-0.3398	-0.3401
-0.4686	-0.4309	-0.4049	-0.4055	-0.3962	-0.3933	-0.3921
-0.4686	-0.4325	-0.4047	-0.4049	-0.3899	-0.2336	-0.3915
-0.4686	-0.4354	-0.3432	-0.4049	-0.3345	-0.3334	-0.3390
0.4204	0.6050	0.6760	0.6681	0.6969	0.6963	0.6901
0.4204	0.5913	0.6760	0.6681	0.6999	0.6938	0.7029
0.4201	0.5905	0.6774	0.6660	0.7568	0.7069	0.7029
0.4201	0.5989	0.6774	0.6660	0.7104	0.6999	0.6898
0.4179	0.6077	0.6768	0.6887	0.6987	0.7013	0.6959
-0.7534	-0.5650	-0.4957	-0.5039	-0.4667	-0.4631	-0.4844

-0.4683	-0.3393	-0.4049	-0.3393	-0.3960	-0.3937	-0.3963
-0.4684	-0.4376	-0.4048	-0.4071	-0.3832	-0.3936	-0.3904
-0.4681	-0.3570	-0.3438	-0.3397	-0.3349	-0.3368	-0.1710
-0.7534	-0.6195	-0.4957	-0.5039	-0.4661	-0.4678	-0.4618
-0.4683	-0.4377	-0.3451	-0.3393	-0.3349	-0.3388	-0.3360
-0.4684	-0.4358	-0.4048	-0.4071	-0.3919	-0.3927	-0.3905
-0.4681	-0.4327	-0.3438	-0.3397	-0.3443	-0.3414	-0.3370
-0.4682	-0.4383	-0.3432	-0.3425	-0.3515	-0.3313	-0.3378
-0.7538	-0.6193	-0.4977	-0.5004	-0.2831	-0.4588	-0.4609
-0.4682	-0.3508	-0.4047	-0.3425	-0.3929	-0.3880	-0.3970
-0.7538	-0.5951	-0.4977	-0.5004	-0.4663	-0.4699	-0.4825
-0.7548	-0.5639	-0.4904	-0.4660	-0.4610	-0.4621	-0.4643
-	0.2924	0.2797	0.2797	0.2602	0.2666	0.2911
-	-	0.2797	0.2797	0.2623	0.2670	0.2646

Table S4. Comparison of energies between the three isomers of [trans-{Cp*Ir}$_2$Nb$_6$O$_{18}$(OCH$_3$)]$^{3-}$

eV	**Isomer I**	**Isomer II**	**Isomer III**
Electrostatic Energy	-416.9272	-416.6600	-415.8545
Kinetic Energy	601.4506	603.2071	602.1887
Coulomb (Steric+OrbInt) Energy	-250.8965	-252.8108	-252.4509
XC Energy	-471.7505	-471.6807	-471.6903
Spin-Orbit ZORA (hartree)	-0.0014385093	-0.0197047913	-0.0014351780
Total Bonding Energy	-538.1235	-537.9444	-537.8069
HOMO (a.u.)	357 A 0.10695817316619E+00	357 A 0.10884879962234E+00	357 A 0.10808034683371E+00

LUMO (a.u.)	358 A 0.20993816832668E+00	358 A 0.20630095167621E+00	358 A 0.19659417795084E+00